Low-altitude atmospheric wind measurement from the combined Mie and Rayleigh backscattering by Doppler lidar with an iodine filter

Zhi-Shen Liu, Dong Wu, Jin-Tao Liu, Kai-Lin Zhang, Wei-Biao Chen, Xiao-Quan Song, Johnathan W. Hair, and Chiao-Yao She

This paper briefly discusses the mobile ground-based incoherent Doppler wind lidar system, with iodine filters as receiving frequency discriminators, developed by the Ocean Remote Sensing Laboratory, Ocean University of Qingdao, China. The presented result of wind profiles in October and November 2000, retrieved from the combined Mie and Rayleigh backscattering, is the first report to our knowledge of wind measurements in the troposphere by such a system, where the required independent measurement of aerosol-scattering ratio can also be performed. A second iodine vapor filter was used to lock the laser to absolute frequency reference for both wind and aerosol-scattering ratio measurements. Intercomparison experiments of the lidar wind profile measurements were performed with pilot balloons. Results showed that the standard deviation of wind speed and wind direction, for the 2–4 km altitude range, were 0.985 m/s and 17.9°, respectively. © 2002 Optical Society of America

OCIS codes: 010.0010, 170.3340, 280.1310, 280.3340, 280.3640, 300.6320.

1. Introduction

The atmospheric wind field can be retrieved from the combined Mie and Rayleigh backscattering by use of an incoherent Doppler lidar. Fabry–Perot interferometers have been used to discriminate the frequency content of the backscattering signal with the fringe imaging technique and the edge technique.[1–4] The relative merits of different Fabry–Perot methods were studied and compared in the literature.[5,6] Since molecular (or atomic) absorption consists of sharp absorption features, a molecular vapor cell can be used as a frequency discriminator, first proposed by Shimizu *et al*.[7] Because an injection-seeded double Nd:YAG pulsed laser outputs single-mode radiation at 532 nm and can be tuned across a number of

iodine (I_2) absorption features, we proposed an incoherent Doppler lidar with a Nd:YAG laser and a I_2 vapor filter to measure the atmospheric wind profiling in 1996,[8,9] and its feasibility was demonstrated.[8–10] Incorporating this concept into a Rayleigh lidar in 1997, Friedman *et al*.[11] first reported results of middle-atmospheric wind measured between 18 and 45 km in altitude, an atmospheric region free from aerosol. While we searched for the best method to measure wind under all atmospheric conditions, it has become more clear that different methods often complement each other. The French Centre National de la Recherche Scientifique group first introduced and demonstrated the symmetric double-edge Fabry–Perot etalon for Doppler lidar wind measurement.[1,12] Independently, the double-edge concept for aerosol wind measurements was demonstrated[13] with two cesium Faraday filters at 852 nm as early as 1991. At about the same time, Korb *et al*.[2,3] began to conduct a series of simulations and studies of the edge technique. Korb *et al*.[14] later concluded that depending on the dominance of aerosol scattering or molecular scattering, the Fabry–Perot etalon with different free spectral range (FSR) should be used, owing to the dramatic difference in the spectral linewidth of the scattering light between the two cases. The linewidth of the former is typically equal to the pulsed laser linewidth, ~100 MHz, and

the latter reflects a Doppler-broadened linewidth of the center peak of Rayleigh scattering, called the Cabannes line,[15] typically 2–3 GHz. It was further suggested that for the aerosol dominated situation, a Nd:YAG laser wavelength at 1064 nm, to suppress Rayleigh scattering, and a narrowband Fabry–Perot with FSR <1 GHz should be used, while the third harmonic of the Nd:YAG laser at 355 nm, to enhance Rayleigh scattering, and a more broadband Fabry–Perot with FSR $\sim$ 10 GHz would be preferred for atmosphere that is dominated by molecular scattering. Gentry *et al.*[16] have recently presented wind measurements with the molecular double-edge technique at 355 nm. The wind-measuring sensitivity is proportional to the slope of the filter transmission at an operating point. The narrowband Fabry–Perot obviously translates to higher wind-measuring sensitivity, and for the edge method it is higher under the aerosol-dominated case. However, under this condition, the edge method is in direct competition with the coherent detection technique.[17]

The use of the second harmonic of Nd:YAG wavelength at 532 nm, with adequate response to both Mie and Rayleigh scattering and a molecular filter as a frequency discriminator with $\sim$ 2 GHz bandwidth, dictated by nature, is a compromise that works well when both scattering components are significant. For the aerosol-dominated situation, the measurement sensitivity of the molecular vapor filter is in general lower, owing to its broader linewidth. However, unlike a Fabry–Perot spectrum, the molecular-absorption band can be made in the shape of a notch. A selected sharp edge of an iodine filter can have a transmission slope that yields wind-measuring sensitivity of $\sim$1% per ms. Although this is a value lower than the theoretical optimum of 8% per ms^{-1} with Fabry–Perot[14] that may be used for the case of exclusive aerosol scattering, it is a respectable value when the signal-to-noise is taken into account, and it is comparable with the Fabry–Perot sensitivity for the molecular-scattering case. There are a number of advantages of molecular filters, including more-stable transmission characteristics, a much wider field of view, and an ease of optical alignment. In addition, perhaps most important for the molecular filter method is its excellent ability to reject aerosol scattering. When operated at a frequency at the center of the absorption notch, the aerosol signal may be attenuated by better than 70 dB, allowing the aerosol-scattering ratio to be measured. The excellent aerosol-rejection capability and the ease of optical alignment of molecular filter had been field tested,[18] and the Wisconsin group replaced Fabry–Perot etalons with an iodine vapor filter in their lidar for the measurement of the aerosol-scattering ratio.[19]

In this paper, a mobile ground-based incoherent Doppler wind lidar (MIDWiL) system is presented for low-altitude atmospheric wind measurements. A unique feature of the MIDWiL system is its capability to monitor the measurement of the aerosol-scattering ratio, with which the radial wind can be determined uniquely from the lidar return. With the aerosol-scattering ratio independently measured, the lidar returns passing through the frequency discriminator can be processed to retrieve Doppler wind profiles under a varied mixture of Rayleigh and Mie scattering. The system was developed by the Ocean Remote Sensing Laboratory (ORSL) of the Ministry of Education of China, Ocean University of Qingdao. The wind profiles were retrieved from the signals of combined Mie and Rayleigh backscattering in October and November 2000. Intercomparison experiments of the lidar wind profile measurements were performed with pilot balloons, and the results are reported.

2. Description of the Instrument

The schematic diagram for lidar transmitter, receiver, and frequency control is shown in Fig. 1. The master of the system is the two-wavelength diode pumped cw single-mode tunable Nd:YAG seed laser. The fundamental output at 1064 nm is used to seed a Continuum Powerlite 7000 Nd:YAG pulsed laser, as shown in the upper part of Fig. 1. The 532-nm output of the seed laser is sent to an iodine filter (cell 1) system in the lower part of Fig. 1 that is used to control and lock the seed laser frequency. By use of this setup, the frequency precision is maintained experimentally to within 0.2 MHz, corresponding to a wind measurement uncertainty of 5.0 cm/s. Whereas the absolute frequency is monitored by iodine absorption, the frequency scale was determined with a monitoring Fabry–Perot with a FSR = 75 MHz, as shown in the bottom of Fig. 1.

The backscattering optical signal is received by a two-mirror scanning system installed on the roof of a container (not shown). The azimuth and zenith scanning are controlled by a stepper motor. The received backscattered light is collected by a Cassegrain telescope with 300-mm aperture, and then passes through a temperature-controlled narrowband Daystar Corporation interference filter (bandwidth = 0.15 nm, peak transmission 35.06%, not shown). As shown in the right of Fig. 1, the collected light is split into two channels; approximately 30% of it is detected directly by a photomultiplier in the reference channel, and the remaining light is passed through an I_2 filter (cell 2) used as a frequency discriminator and then detected by a second photomultiplier in the measurement channel. EMI9214B PMTs with gating control are used, and the signals from the two channels are digitalized by a dual channel 40-MHz, 12-bit analog-to-digital converter.

Absorption line No. 1109 of the iodine[20] is selected for use in this lidar system. Under the operating conditions, its normalized transmission function, detailed in Section 3, is shown in Fig. 2. For wind measurement, the absorption spectral profile of the I_2 molecular filter needs to be very stable. The detection iodine cell, which is stabilized through control of
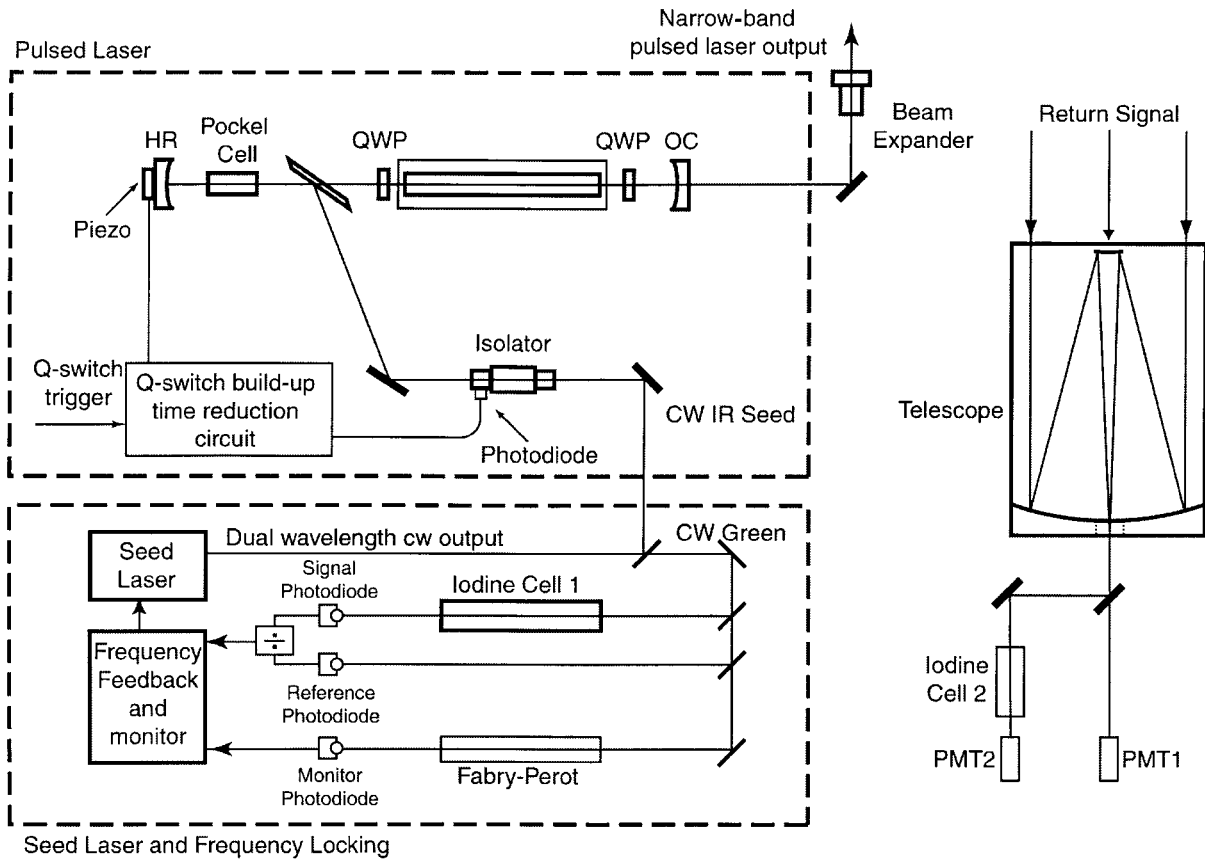
Fig. 1. Schematic diagram for injection-seeded Q-switched pulsed Nd:YAG laser transmitter on the left panels. The lidar receiver is shown on the right, where the iodine cell 2 is the frequency discriminator.

the temperature of the cell body and cell finger separately, has been constructed and found to have long-term stability. Since the vapor density is more sensitive to change in iodine vapor pressure, the temperature of the cell finger is controlled to near 65 °C within 0.01 °C rms, while its cell body is near 70 °C within 0.1 °C. The resulting transmission curve for the vapor filter near 532 nm is shown in Fig. 2, where the absorption line center at 18787.796 cm^{-1} is marked A as zero reference in the frequency scale for convenience. For wind measurement, the laser frequency is tuned to the half-level point on edge of I$_2$ normalized transmission, point E, and locked there by electronic feedback. The absolute frequency of the locking point, E, is 18787.830 cm^{-1}, which is 1.020 GHz higher in frequency than the well center A. For measuring the aerosol scattering ratio, the green seed light is tuned to the point A in Fig. 2. The parameters of MIDWiL system are summarized in Table 1.

3. Method

It is straightforward to show that the detected photoncounts at a range r in the total scattering reference channel, N_R, and in the measurement channel

N_M are given in Eqs. (1a) and (1b), adopted from Hair et al.[21]:

$$N_R = k_R \left(\frac{\Delta r}{r^2} \right)(\beta_a + \beta_m)\exp\left\{ -2 \int dr[\alpha_a(r') + \alpha_m(r')] \right\}, \tag{1a}$$

$$N_M = k_M \left(\frac{\Delta r}{r^2} \right)(f_a\beta_a + f_m\beta_m)\exp\left\{ -2 \int dr[\alpha_a(r') + \alpha_m(r')] \right\}. \tag{1b}$$

Here, Δr is the range resolution; β_a and β_m (α_a and α_m) are aerosol and molecular volume backscatter (extinction) coefficients, respectively; and k_R and k_M are the system constants for reference and measurement channel, respectively, depending on total laser emission energy and the efficiency of each optical and electronic component.

When there is nonzero line-of-sight wind with velocity V_R (assuming the direction opposing the transmitting laser to be positive), the frequency of the

Iodine Transmission, Line 1109
I₂ cell finger: 65.02 °C; I₂ cell body: 69.8 °C
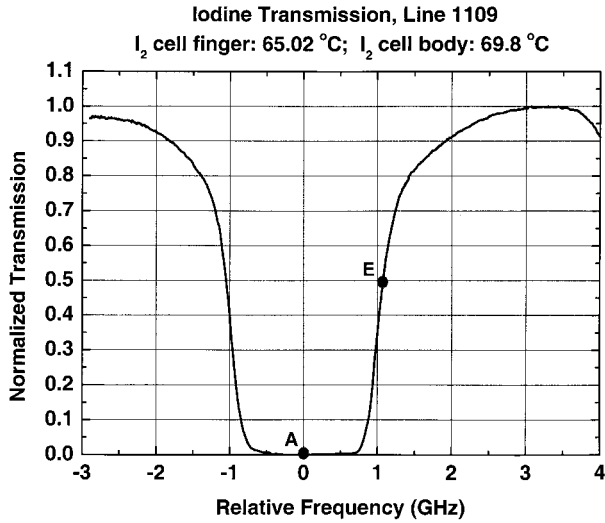
Fig. 2. Normalized transmission for absorption line 1109 of the iodine filter near 532 nm. The temperature of cell finger and cell body are 65.02 °C and 69.8 °C, respectively. The wave numbers at reference point A and locking point E are 18787.796 and 18787.830 cm^{-1} (1.02 GHz apart), respectively.

received light, ν, is Doppler shifted by $\Delta\nu_D = (2V_R/\lambda)$ from transmitting frequency ν_0; the parameters in Eqs. (1a) and (1b) are a function of ν as

$$f_a(\nu) = F(\nu), \qquad (2a)$$

$$f_m(T, P, \nu) = \int \Re(\nu' - \nu, T, P)F(\nu')d\nu', \quad (2b)$$

$$\int \Re(\nu' - \nu, T, P)d\nu' = 1, \qquad (2c)$$

which are, respectively, the aerosol attenuation factor due to iodine filter at the receiving frequency $\nu = \nu_0 + \Delta\nu_D$, the attenuation factor for Cabannes–Brillouin scattering[15,21] by the iodine filter, and the expression showing that the normalized Cabannes–Brillouin scattering function,[21] $\Re(\nu, T, P)$ is used here. $F(\nu)$ is the transmission function of the iodine filter for the return signal; it is convolution of the measured (cw) iodine filter function and laser lineshape function.

There are several linear regions in iodine transmission curves, each of which may be used as a frequency discriminator for wind measurements. We use the transmission function of the I₂ 1109 line, normalized to the maximum transmission, as shown in Fig. 2. The line-of-sight (or radial) wind velocity V_R may be determined through a proper processing of the measured wind ratio of the lidar returns,

$$R_W(\nu) = \frac{N_M(\nu)}{N_R(\nu)} = \frac{k_M}{k_R}\left[\frac{f_a(\nu)(\beta_a/\beta_m) + f_m(\nu)}{(\beta_a/\beta_m) + 1}\right], \quad (3a)$$

Transmitter	Parameter
Wavelength (nm)	532
Repetition rate (Hz)	30
Pulse energy (mJ)	200
Pulse duration (ns)	8
Pulsed laser linewidth (MHz)	100

Receiver	Parameter
Telescope aperture (mm)	300
Field of view (mrad)	2.0
Focal length of the telescope (mm)	700
Interference filter bandwidth (nm)	0.15
Peak transmission of the interference filter	35.06%
Dimension of iodine-vapor filter (mm)	20 (dia.); 106 (length)
Detector (photo-multiplier PMT)	EMI 9214B
Pulse rise time (ns) of PMT	2.0

where $\nu = \nu_0 + \Delta\nu_D$. Since at zero wind the wind ratio is

$$R_W(\nu_0) = \frac{N_M(\nu_0)}{N_R(\nu_0)} = \frac{k_M}{k_R}\left[\frac{f_a(\nu_0)(\beta_a/\beta_m) + f_m(\nu_0)}{(\beta_a/\beta_m) + 1}\right], \quad (3b)$$

a normalized wind ratio (NWR) may be defined as NWR $= R_W(\nu)/2R_W(\nu_0)$, and it is a function of $\Delta\nu_D = \nu - \nu_0$, or in turn a function of V_R,

$$\text{NWR} = \frac{R_W(\nu)}{2R_W(\nu_0)} = 0.5\left[\frac{f_a(\nu)(\beta_a/\beta_m) + f_m(\nu)}{f_a(\nu_0)(\beta_a/\beta_m) + f_m(\nu_0)}\right]. \quad (3c)$$

The factor of 2 in the denominator is there to ensure that NWR = 0.5 under zero-wind condition. To make use of Eqs. (3a)–(3c) for lidar retrieval of line-of-sight wind from lidar returns, N_M and N_R, we need to know the parameters and functions on the right-hand side of the equations. One can measure the constant k_M/k_R by removing the filter from the system, and the functions f_m and f_a can be determined from the measured absolute transmission spectrum of the iodine filter, $F(\nu)$, and the molecular scattering spectrum, $\Re(\nu, T, P)$ with temperature and pressure profiles obtained from a standard atmospheric model or local rawinsondes. The aerosol-scattering ratio, $R_b = (\beta_a/\beta_m)$, needs to be determined independently.

It should be noted that due to passive window losses and the presence of continuum absorption,[21] the measured maximum (at a frequency away from absorption features) filter transmission is less than unity. An alternative, and perhaps conceptually simpler, approach is to normalize the maximum iodine transmission within the frequency range of interest to unity, as is done for Fig. 2. In this approach, we take the function, $F(\nu)$, as the normalized filter transmission, which is then used to calculate $f_m(\nu)$ and $f_a(\nu)$ for Eqs. (3a) and (3b). The measured absolute maximum filter transmission is then absorbed into the factor k_M. Since the calibration curves, NWR of Eq. (3c), is independent of k_M/k_R,

Atmosphere Temperature 255.7K, Altitude ~5km

(a)

Atmosphere Temperature 238.2K, Altitude ~7km

(b)
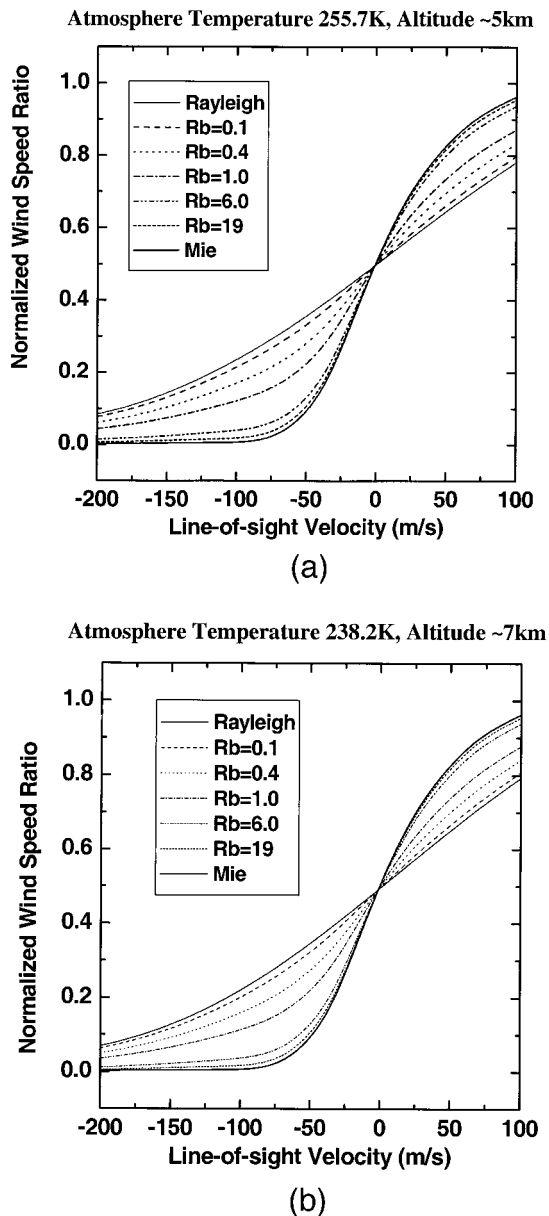
Fig. 3. NWR as a function of line-of-sight wind velocity with different aerosol scattering ratio, R_b. The aerosol scattering ratio for pure Rayleigh case is $R_b = 0$. (a), atmosphere temperature of 255.7 °K (altitude ~5 km), (b) atmosphere temperature of 238.2 °K (altitude ~7 km).

and $f_m(v)$ and $f_a(v)$ appear in both numerator and denominator, the NWR is independent of which way we interpret the filter transmission function, $F(v)$. Unless both $N_M(v)/N_R(v)$ and $N_M(v_0)/N_R(v_0)$ are determined simultaneously through the same detection system, care is needed to define and determine k_M/k_R and $F(v)$ consistently for the application of Eq. (3a) and/or Eq. (3b).

For a given aerosol-scattering ratio, R_b and filter function $F(v)$, the NWR may be calculated from Eq. (3c), resulting in calibration curves for different R_b, shown in Fig. 3. Experimentally, one determines $R_W(v)$ from lidar returns by Eq. (3a). The needed

$R_W(v_0)$ may be calculated either from the measured filter function and aerosol-scattering ratio or by real-time normalization measurement, injecting a small amount of elastically scattered light (by means of a coupling fiber, for example) into the same receiving system.[3] Comparing the measured NWR = $R_W(v)/2R_W(v_0)$ to the calculated curves shown in Fig. 3, the line-of-sight wind can then be determined. Since the NWR, strictly speaking, is dependent on the atmospheric temperature, for the purpose of wind retrieval we have calculated a lookup table of NWR that covers the range of possible tropospheric temperatures, corresponding to a maximum wind speed error of 2 m/s. If the standard atmospheric temperature is then assigned according to the altitude for the determination of wind components, then we can extract the wind component from the lookup table with a wind-speed error less than 1 m/s. In Fig. 3, we present the calibration curves, NWR versus line-of-sight velocity for two different temperatures [$T = 255.7$ °K for altitude ~5 km and $T = 238.2$ °K for altitude ~7 km, in Figs. 3(a) and 3(b), respectively], each with seven values of R_b. Notice for the Mie scattering case, $R_b = \infty$, the slope is sharpest, corresponding to a measurement sensitivity of ~0.8% per ms^{-1}.

As shown in Fig. 3, the retrieval of line-of-sight wind velocity V_R depends on an independent knowledge of aerosol scattering ratio R_b. We can measure the aerosol backscattering ratio,[7] $R_b + 1$ using the same MIDWiL system by locking the frequency of the injection-seeded laser to the point A at the 1109 line center of the I$_2$ filter, where the aerosol backscattering will be mostly absorbed by the filter (measured to be 70 dB). Setting $f_a = 0$ in Eq. (1b), we can express the atmospheric aerosol-scattering ratio R_b as

$$R_b(r) = \frac{\beta_a(r) + \beta_m(r)}{\beta_m(r)} - 1 = \frac{k_M f_m N_R(r)}{k_R N_M(r)} - 1. \quad (4)$$

In this manner, the aerosol scattering ratio R_b can be measured with an accuracy better than 10%. The simulation (Fig. 3) shows that the uncertainty of line of sight (LOS) wind speed is less than 0.2 m/s when R_b is in range of 6–19 and is less than 0.8 m/s when R_b is in range of 0.1–0.4 for a backscatter ratio (or aerosol-scattering ratio) measured with the accuracy better than 10%. Figure 4 shows an example of a backscatter ratio measured on 30 October 2000, in Qingdao, China. Since the aerosol condition usually does not change rapidly, one needs to measure such a profile only once in several hours, unless a frontal event is under consideration.

For the wind measurements, the Doppler lidar is operated at a zenith angle of 30° or 15°. Two opposing off-vertical measurements at a given zenith angle on a plane with a given azimuth angle can give a horizontal wind velocity. If v_+ and v_- are the LOS velocities of the off-vertical measurements with a ze-
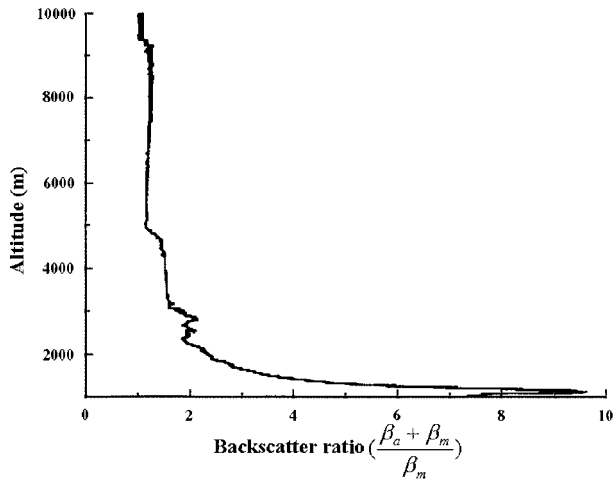
Fig. 4. Example of backscatter ratio, $(\beta_a + \beta_m)/\beta_m = R_b + 1$, measured on 30 October 2000 in Qingdao, China.

nith angle θ at range r, the relationship between the different components can be written as

$$\nu_+ = \nu_h \sin \theta + \nu_\nu \cos \theta,$$
$$\nu_- = -\nu_h \sin \theta + \nu_\nu \cos \theta, \qquad (5)$$

where, ν_h is the horizontal wind velocity at a given azimuth and ν_ν is the vertical wind velocity. Therefore the horizontal velocity can be obtained:

$$\nu_h = \frac{\nu_+ - \nu_-}{2 \sin \theta}. \qquad (6)$$

If two horizontal wind velocities of different azimuth angles are obtained, the horizontal wind vector can be calculated based on the relationships in trigonometry.

4. Experimental Results, Comparisons, and Discussion

Seven intercomparison experiments of our lidar wind profile measurements were performed with pilot balloons in October and November 2000 at ORSL near the Qingdao meteorological station (QMS). The data of the pilot balloon were collected by a rawinsonde system, and the balloons were launched a horizontal distance of 400 m from our lidar at Ocean University of Qingdao. For the measurements shown in Figs. 5 and 6, the rising rate of balloon was approximately 5.0 m/s, and its maximum detection altitude was 10 km. The data profile had 17 sampling altitudes, which were 0, 0.385, 0.50, 0.685, 0.985, 1.0, 1.5, 2, 3.0, 4.0, 5.0, 5.5, 6.0, 7.0, 8.0, 9.0, and 10 km, respectively. The range resolution of lidar was 150 m. The altitude range of balloon and lidar measurements cover from 100 m to 7 km. Ten independent laser profiles were obtained in 10 min; each profile of wind speed and direction was derived from the lidar Doppler shift measurements of LOS taken at an zenith angle of 30° or 15°. Each LOS wind measurement was determined from 1000-laser
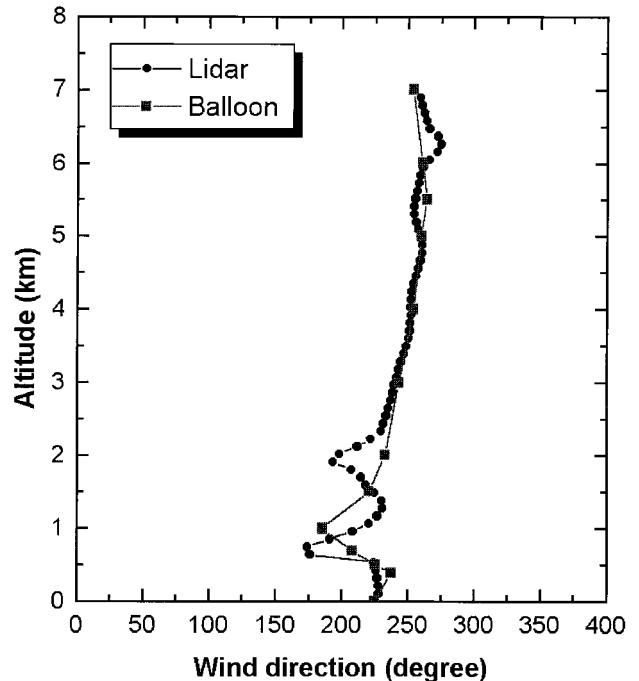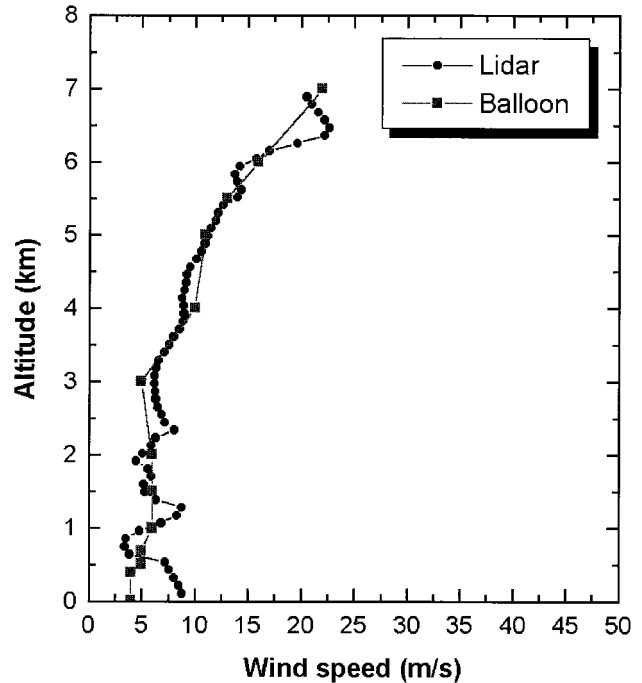
Fig. 5. Measurements of wind speed and direction by rawinsonde balloon of Qingdao Meteorological Station (QMS) and ORSL lidar from 8:00 PM to 9:00 PM on 30 October 2000. Filled circle, lidar data; filled diamond, collocated rawinsonde data. The angle indicating wind direction is zero for south-pointing wind and increases as it rotates toward the west.

pulses (about 1.5 minutes) averaged to better match the time scale of the balloon.

Figure 5 shows wind speed and direction measurement results from the rawinsonde balloon of QMS and our lidar nearby from 8:00 PM to 9:00 PM on 30 October 2000. The wind-speed maximum for the
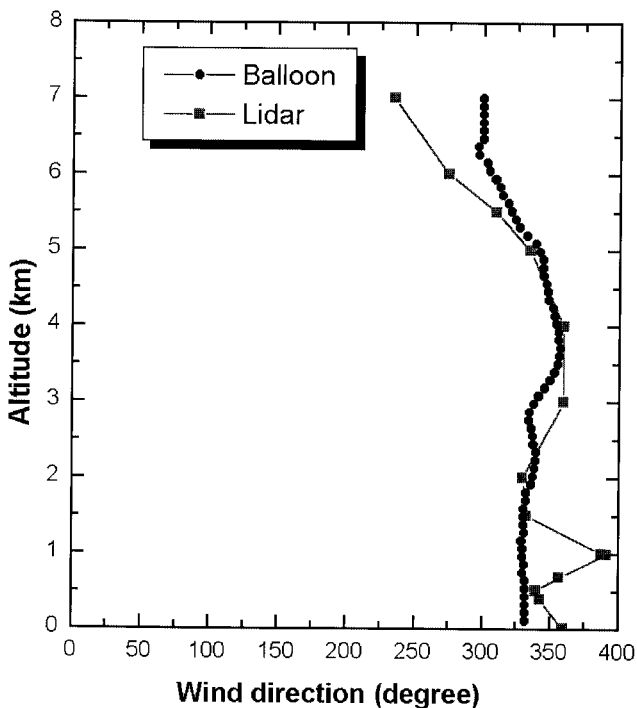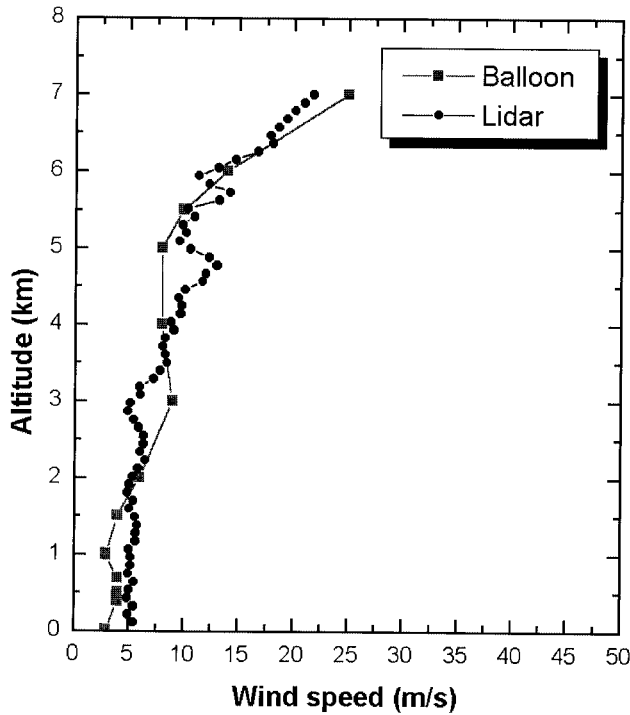
Fig. 6. Wind and direction profiles measured by QMS rawinsonde balloon and ORSL lidar from 8:00 PM to 9:00 PM on 1 November 2000. Filled circle, lidar measurement data; filled diamond, collocated rawinsonde data. Wind direction convention is the same as in Fig. 5.

Fig. 7. Comparison between lidar wind and balloon wind between 2 and 4 km for all seven experiments. The standard deviations of wind speed and direction are 0.985 m/s and 17.9°, yielding correlation coefficients 0.96 and 0.95, respectively.

wind shear. The standard deviation of wind speed is 1.2 m/s and that of wind direction is 18°. From Fig. 5, we note that wind speed and direction have appreciable deviations at the altitude range from 0.8 to 2.5 km from the balloon data. The higher spatial and temporal resolution of lidar measurements suggests its potential use for boundary layer studies. Figure 6 shows the results of another measurement taken from 8:00 PM to 9:00 PM on 1 November 2000. The wind speed ranged from 5 to 22 m/s with increasing altitude. The wind direction was south. The wind speeds are in general agreement. The wind directions at 1 and 7 km had a difference of about 60° between lidar and balloon measurements, which could be due to the spatial differences, since the balloon and lidar were not exactly colocated as the balloon ascended.

The comparison between lidar data and simultaneous pilot balloons data of seven experiments in the region from 2 to 4 km altitude is shown in Fig. 7. The standard deviations of wind speed and wind direction are 0.985 m/s and 17.9°, respectively, in this

profile was 22 m/s. The wind direction was northeast and increased in magnitude with altitude. A variation on wind vectors around altitudes between 0.5 and 2.5 km shown in the right figure is due to

altitude region. We also calculated the standard deviations of lidar wind speed and direction from balloon data in the region below 2 km in altitude (1.515 m/s and 22.3°, respectively). As expected, the standard deviation of wind speed and direction in the region between 2 and 4 km is better than those below 2 km, where the spatial difference between the balloon and lidar location has a more significant effect.

In conclusion, a mobile ground-based incoherent Doppler wind lidar (MIDWiL) system was developed by Ocean Remote Sensing Laboratory of the Ministry of Education of China, Ocean University of Qingdao (OUQ), and the wind profiles in October and November 2000 were retrieved from the combined signals of Mie and Rayleigh (really Cabannes–Brillouin) backscattering together. The iodine vapor filter was used to lock the transmitting laser frequency as well as required frequency discriminator for the receiver. A unique feature of this lidar lies in its capability for an independent measurement of aerosol scattering ratio, with which the radial wind can be determined uniquely from the lidar return. This permits the frequency discriminator of lidar to process Doppler shift resulting from a varied atmospheric aerosol content. Comparison experiments between lidar wind profile measurements and those with pilot balloons were performed, resulting in a standard deviation of 0.985 m/s in wind speed and of 17.9° in wind direction. Our lidar system worked well in the region where both the aerosol and Rayleigh scattering are important.

References

1. M. L. Chanin, A. Gariner, A. Hauchecorne, and J. Porteneuve, "A Doppler lidar for measuring winds in the middle atmosphere," Geophy. Res. Lett. **16,** 1273–1276 (1989).
2. C. L. Korb, B. Gentry, and C. Weng, "The edge technique: theory and application to the lidar measurement of atmospheric winds," Appl. Opt. **31,** 4202–4213 (1992).
3. C. L. Korb, B. Gentry, and X. Li, "Edge technique Doppler lidar wind measurements with high vertical resolution," Appl. Opt. **36,** 5976–5983 (1997).
4. K. F. Fischer, V. J. Abreu, W. R. Skinner, J. E. Barnes, M. J. McGill, and T. D. Irgang, "Visible wavelength Doppler lidar for measurement of wind and aerosol profiles during day and night," Opt. Eng. **34,** 499–511 (1995).
5. J. A. McKay, "Modeling of direct detection Doppler wind lidar. I. The edge technique," Appl. Opt. **37,** 6480–6486 (1998).
6. J. A. McKay, "Modeling of direct detection Doppler wind lidar. II. The fringe imaging technique," Appl. Opt. **37,** 6487–6493 (1998).
7. H. S. Shimizu, A. Lee, and C. Y. She, "High spectral resolution lidar system with atomic blocking filters for measuring atmospheric parameters," Appl. Opt. **22,** 1373–1391 (1983).
8. Z. S. Liu, W. B. Chen, T. L. Zhang, J. W. Hair, and C. Y. She, "Proposed ground-based incoherent Doppler lidar with iodine filter discriminator for atmospheric wind profiling," in *Application of Lidar to Current Atmospheric Topics*, A. J. Sedlacek, ed., Proc. SPIE **2833,** 128–135 (1996).
9. Z. S. Liu, W. B. Chen, T. L. Zhang, J. W. Hair, and C. Y. She, "An incoherent Doppler lidar for ground-based atmospheric wind profiling," Appl. Phys. B **64,** 561–566 (1997).
10. W. B. Chen, T. L. Zhang, D. Wu, and Z. S. Liu, "Atomic filter for laser Doppler velocimetry," Acta Opt. Sin. **17,** 346–350 (1997), (in Chinese).
11. J. S. Friedman, C. A. Tepley, P. A. Castleberg, and H. Roe, "Middle-atmospheric Doppler lidar using an iodine-vapor edge filter," Opt. Lett. **22,** 1648–1650 (1997).
12. A. Garnier and M. L. Chanin, "Description of a Doppler Rayleigh LIDAR for measuring winds in the middle atmosphere," Appl. Phys. B **55,** 35–40 (1992).
13. S. H. Bloom, R. Kremer, P. A. Searcy, M. Rivers, J. Menders, and E. Korevaar, "Long-range, noncoherent laser Doppler velocimeter," Opt. Lett. **16,** 1794–1796 (1991).
14. C. L. Korb, B. M. Gentry, S. X. Li, and C. Flesia, "Theory of the double-edge technique for Doppler lidar wind measurement," Appl. Opt. **37,** 3097–3104 (1998).
15. C. Y. She, "Spectral structure of laser light scattering revisited: bandwidths of nonresonant scattering lidar," Appl. Opt. **40,** 4875–4884 (2001).
16. B. M. Gentry, H. Chen, and S. X. Li, "Wind measurements with 355-nm molecular Doppler lidar," Opt. Lett. **25,** 1231–1233 (2000).
17. R. T. Menzies, "Doppler lidar atmospheric wind sensors: a comparative performance evaluation for global measurement applications from earth orbit," Appl. Opt. **25,** 2546–2553 (1986).
18. R. J. Alvarez II, L. M. Caldwell, Y. H. Li, D. A. Krueger, and C. Y. She, "High spectral resolution lidar measurement of tropospheric backscatter-ratio using barium atomic blocking filter," J. Atmos. Oceanic Tech. **7,** 876–881 (1991).
19. P. Piironen and E. W. Eloranta, "Demonstration of a high-spectral-resolution lidar based on an iodine absorption filter," Opt. Lett. **19,** 234–236 (1994).
20. S. Gerstenkorn and P. Luc, "Atlas du spectre d'absorption de la molecule d'iode," (Centre National de la Recherché Scientifique, Paris. 1978).
21. J. W. Hair, L. M. Caldwell, D. A. Krueger, and C. Y. She, "High-spectral-resolution lidar with iodine-vapor filters: measurement of atmospheric-state and aerosol profiles," Appl. Opt. **40,** 5280–5294 (2001).